A Filter Design Method for Minimizing Ringing in a Region of Interest in MR Spectroscopic Images

Tariq Bakir and Stanley J. Reeves*

Abstract—**Magnetic resonance spectroscopic imaging (MRSI) requires a relatively long time to sample k-space (the spatial frequency domain), effectively lowpass filtering the resulting reconstructed image. Ringing is especially problematic when a region of interest (ROI) is close to a bright region outside the ROI, since the bright region tends to create a ringing artifact into the ROI due to the lowpass nature of the data. In this paper, we propose a method that reduces the effect of a stronger signal region on a weaker signal in a nearby ROI by designing a postprocessing filter that steers the strong interference away from the ROI. The proposed method is computationally simple both in the design stage and in applying it to images. We present experiments that illustrate the value of the technique.**

Index Terms—**Blur, interpolation, ringing reduction, spectroscopic imaging.**

I. INTRODUCTION

A. Problem Description

IN MANY TYPES of medical imaging, the available resolution does not allow one to separate regions of interest from the interference of nearby signal energy that is not of interest. This problem is especially acute in some types of MRI. In particular, MR spectroscopic imaging (MRSI) requires a relatively long time to sample k-space (the spatial frequency domain) [1].

Spectroscopic imaging techniques are hybrid techniques combining the ability of NMR spectroscopy to identify and measure biochemical consituents with the ability of MR imaging to localize these signals and thereby form useful maps of anatomy. Thus, MRSI can present information in the form of maps representing not simply anatomy, but representing local metabolic states [2], or local tissue abnormalities. As a result of this capability, MRSI has been proposed as a method to localize and assess brain tumors [3] and multiple sclerosis [4] as well as to determine the seizure focus of temporal lobe epilepsy [5]. These spectroscopic imaging techniques are useful only to the extent that they can clearly represent local differences among tissue types; for example, they must have sufficient spatial resolution to resolve the spectrum of heart muscle from
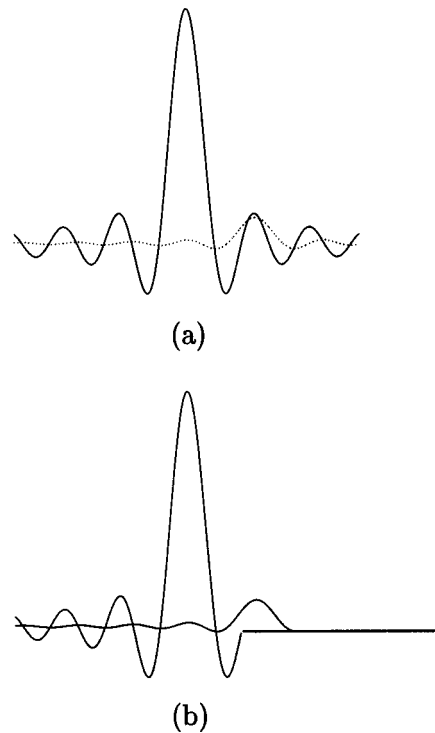
Fig. 1. (a) Impulses observed after LPF and (b) impulses observed after idealized postprocessing.

the spectrum of the blood within the neighboring ventricular chambers.

Since only a limited region of the spatial-frequency domain can be sampled, the image is effectively lowpass filtered by the acquisition method. The ringing caused by this lowpass filtering is especially problematic if the signal intensity from one region is much stronger than a nearby region of interest (ROI). The tails of the point-spread function (PSF) ring and decay over a broad area, causing the strong unwanted signal to appear in the ROI and thereby making it difficult to interpret the image in the ROI.

In essence, the goal of this work is to minimize the effects of ringing of one region into another. The potential benefits of this are both visual and analytical. Some applications require that an ROI be viewed where there is ringing caused by interference from nearby regions with strong intensity. This makes visual assessment difficult in the ROI. In other applications, the ultimate goal is not to view an image but rather to measure the concentration of some chemical in a specified region. This region may be close to an unwanted signal that rings into the ROI and interferes with the measurement process. In this case we desire a
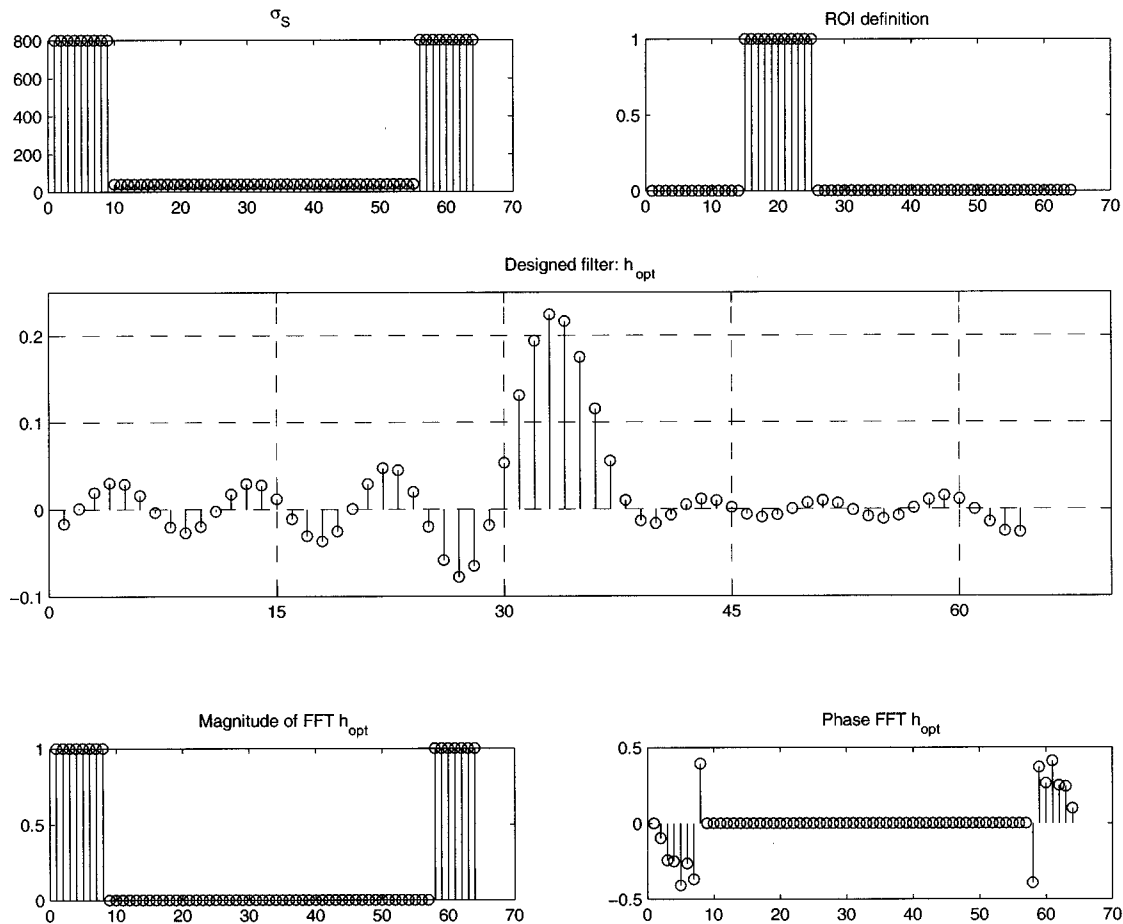
Fig. 2.   1-D Uncorrelated model with nonlinear constraint.

filter that allows a better approximation of the true concentration in the specified region. Measuring the concentration of a particular chemical in a specified ROI in the brain from MRSI images is being used increasingly as a tool in the treatment of diseases such as epilepsy and other disorders that manifest certain biochemical anomalies [5].

The problem of reducing the ringing in an image has been addressed in several ways. Some methods use prior knowledge about an image. For example, if the image is known to have a finite spatial region of support (ROS), it is possible to reduce ringing by extrapolating the missing higher frequencies [6]. The problem with this method is that most of the improvement is near the boundary of the spatial ROS and it is computationally expensive. Other researchers have used prior information from a high-resolution MRI scout to obtain a model for the corresponding spectroscopic image. The earliest of these, spectral localization by imaging (SLIM), modeled the data as homogeneous compartments whose shape was derived from a corresponding MR proton density image [7]. Extensions of this idea have also been proposed [8], [9]. These methods require the availability of a high-resolution scout image, and the resulting reconstructions are somewhat sensitive to errors in the model used. Another approach attempts to account for the presence of edges in images by using adaptive regularization or Bayesian methods, such as in [10]. These methods generally model the image as smooth regions with edge-like boundaries.

The modeling determines where edges fall in an attempt to reduce the blurring across them and associated ringing artifacts. These methods are powerful but are computationally expensive. Furthermore, artifacts can be quite severe even with small errors in the locations of boundaries. The resulting images are also sometimes difficult to interpret.

In the next section, we formulate the ringing minimization problem as a filter design problem, propose an optimization algorithm, and demonstrate the method with simulations. In Section III, we extend the method to the problem of estimating concentration in a region and demonstrate the method using simulations. In Section IV, we present results using real image data. We discuss our results and draw conclusions in Section V.

II. BASIC DESIGN METHOD

We desire a way to minimize the ringing of the stronger unwanted signal into the weaker signal ROI. The solution we propose is motivated primarily by problems in MRI and MRSI; however, the solution is applicable to any kind of low-resolution image that needs to be interpolated for viewing an ROI without interference from a strong nearby signal. In essence, we propose to design a postprocessing filter that modifies the PSF so that the tails of the PSF steer the ringing from the interfering signal away from the ROI. As in all filter design problems, this strategy involves a tradeoff. We reduce the ringing from a large nearby
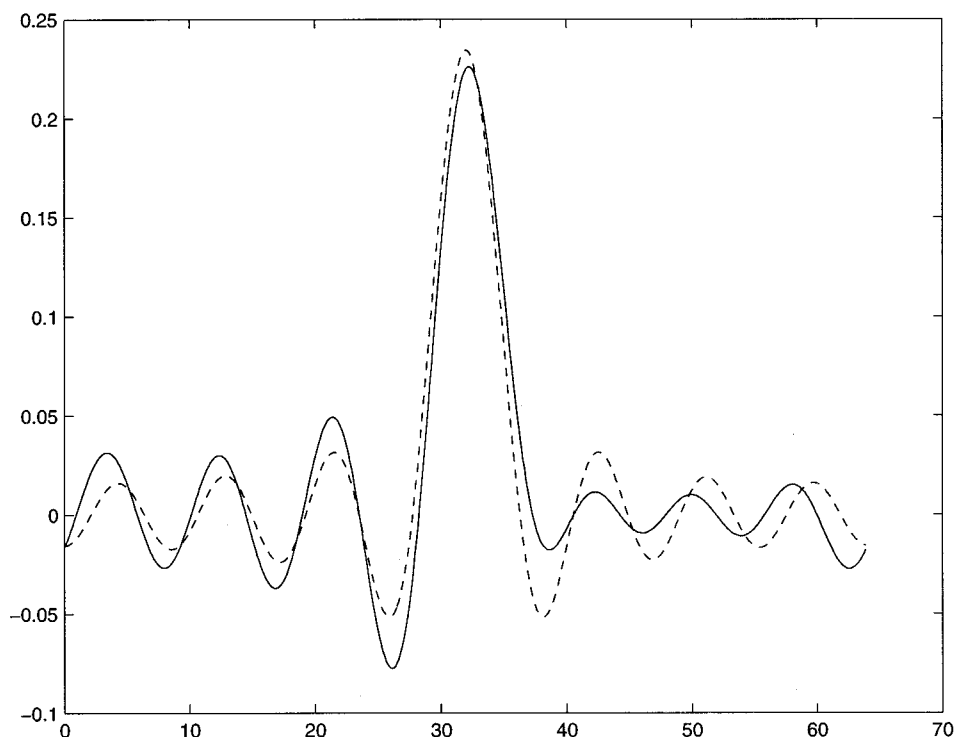
Fig. 3. Comparison of original and optimized PSF—original = dashed, optimized = solid.

signal in one place at the expense of allowing more ringing from other places where the signal is not as strong. This allows us to reduce the overall error in the ROI.

This idea is illustrated in Fig. 1. Suppose we are interested in the strength of a small impulsive signal to the right of a much larger impulsive signal that is not of interest. Due to the bandlimited imaging process, the resulting image will be a superposition of two sinc functions, shown in Fig. 1(a). The first sidelobe to the right of the large signal is so large that it obscures the true strength of the signal on the right. Suppose, however, that through postprocessing methods the overall PSF could be reshaped to eliminate sidelobes on the right. Then the two constituent signals would appear as in Fig. 1(b). In this case, the large signal no longer generates interfering sidelobes, and the strength of the smaller signal of interest can be observed clearly. The goal of our method is to suppress interfering sidelobes as much as possible using a simple postprocessing method but without necessarily sacrificing overall resolution, as is the case when the frequency response is merely apodized.

Our method assumes that the ROI can be specified before designing the filter and that we know something about the relative expected local signal and noise strength. While this information is necessary for the proposed method, the resulting design is rather insensitive to small errors in the prior information used; that is, the optimality of the design degrades slowly as errors are introduced into the prior information. Therefore, we can apply the technique when we only have a general idea where the strong signal is and how strong it is relative to the signal in the ROI. We will demonstrate this claim later in our simulations. Also, as long as the noise is relatively small compared to the signal, the resulting design is only slightly affected by the noise variance assumed [13].

A. Criterion

We model the observed image data as:

$$d = (s + u) * h_0 \tag{1}$$

where s is the high-resolution image observed by the measurement process, u is white measurement noise, and h_0 is a filter expressing the bandlimiting operation associated with the imaging process. The operation $x * y$ in this context denotes convolution of the image represented by the vector x with the image represented by the vector y. Both the observed signal and noise are equally bandlimited by the imaging system. Therefore, the filter h_0 is applied to both.

The filter design problem is based on the definition of a mean square error (MSE) criterion for the error that is caused by the ringing and blurring in the ROI. The resulting quadratic cost formulation is straightforward to minimize and is easily modified for various situations that we discuss later. The problem can be formulated as a constrained optimization problem as follows:

$$\min_h E[||d * h - s||^2] \text{ over ROI} \quad \text{subject to } h \in \Omega \tag{2}$$

where h is the filter to be designed. The filter h is constrained to have the same ROS as h_0 in the frequency domain. This allows us to simplify (2) to:

$$\min_h E[||(s + u) * h - s||^2] \text{ over ROI} \quad \text{subject to } h \in \Omega \tag{3}$$

The equation above can be written in a more convenient form by grouping similar terms and showing the explicit dependence on the ROI. We accomplish this by defining a binary mask $w(n)$
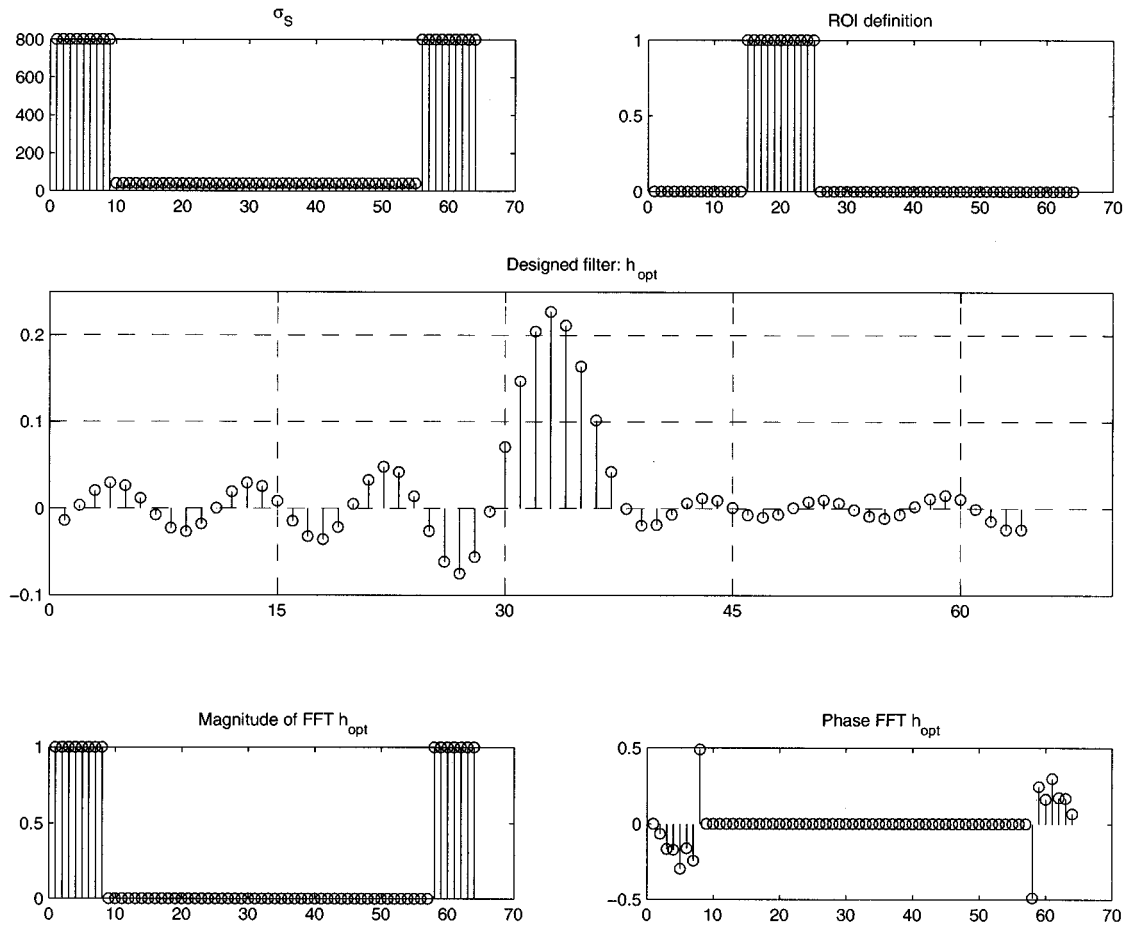
Fig. 4. Correlated model effect on designed filter.

that selects only the ROI and zeros out everything outside the ROI. Thus, the error becomes

$$\phi(h) = \sum_n w(n) E[\{[h(n) - \delta(n)] * s(n)\}^2 \\ + [h(n) * u(n)]^2 + 2\{[h(n) - \delta(n)] * s(n)\} \\ \times \{h(n) * u(n)\}]. \qquad (4)$$

The minimum for the unconstrained problem occurs when $h(n) = \delta(n)$. This means the constrained problem can be interpreted as matching h to an impulse as closely as possible according to the weighting above while satisfying the frequency-domain ROS constraint. (This viewpoint is later generalized when we discuss the concentration measurement problem.) Since intuitively we are trying to match h to an impulse with (ordinarily) a lowpass frequency constraint imposed, h is expected to have a shape similar to a sinc function but with smaller lobes oriented in the relative direction of the ROI from the direction of the large interfering signal nearby. We treat two possible cases for the constraint Ω:

1) The magnitude may be constrained to be an ideal lowpass filter (LPF) with unity gain in the ROS. This is a nonlinear constraint since it can not be implemented in terms of convolutions.

2) The magnitude of the Fourier transform may be constrained to be zero outside the ROS with no constraint inside the ROS. This is a linear constraint since the constraint can be implemented as a bandlimiting operator h_0 convolved with the filter to be designed.

In terms of clinical applications, the nonlinear constraint provides a more generally applicable design. The nonlinear constraint may be used in a wider variety of problems since it does not modify the acquired data as drastically (does not attenuate any components because of the unity gain requirement). Furthermore, it makes the design less sensitive to the prior information about the relative variances of different parts of the image. In both cases, (4) is used but with the appropriate constraint imposed.

B. Algorithm

The conjugate gradients (CG) method was used as the basis for the optimization algorithm because of its ease of implementation and speed of convergence. Unfortunately, the problem formulated in (3) is a constrained optimization problem for which standard CG is inappropriate. However, CG can be modified to incorporate constraints by using the projection method. The projection method involves writing the iteration as an unconstrained iteration but projecting the unconstrained update at each iteration onto the set of feasible solutions
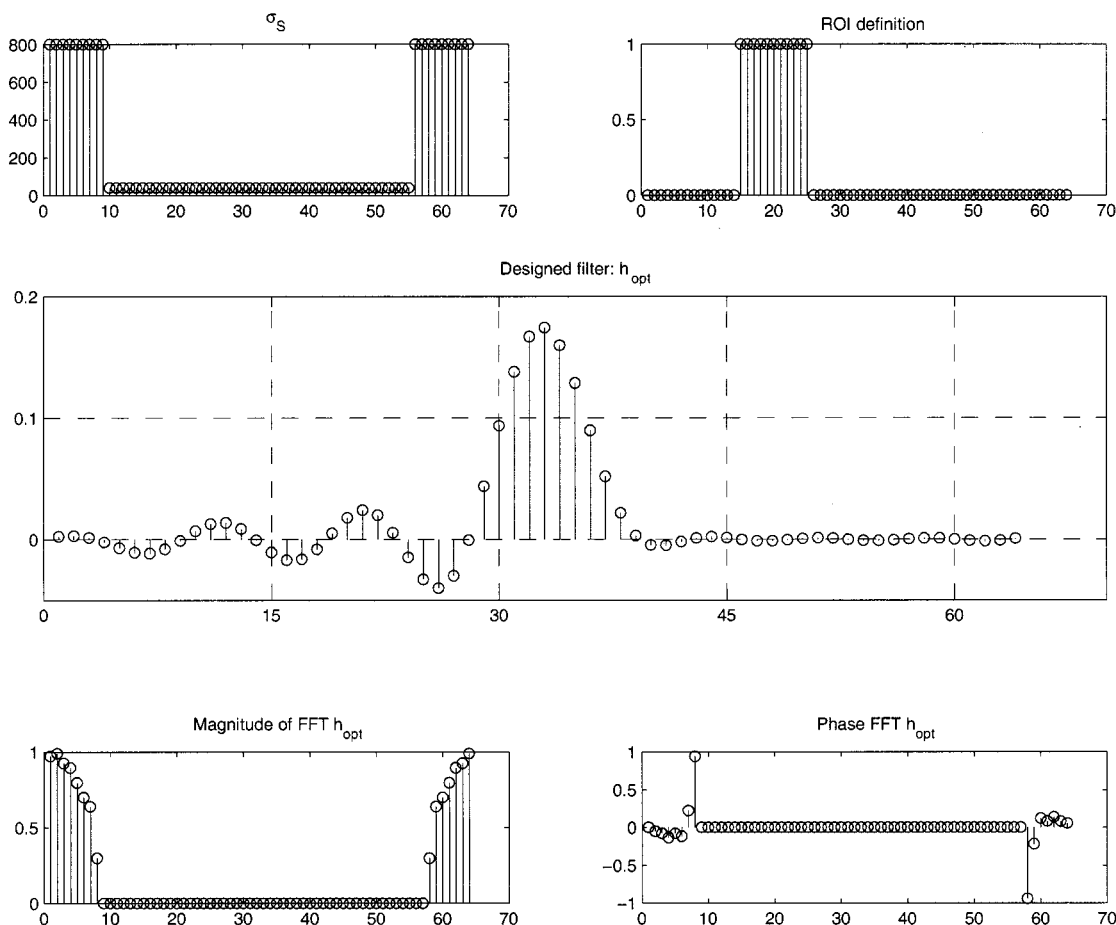
Fig. 5.   Linear constraint effect.

using a projection operator P [11]. If we merely constrain the frequency response to be zero outside the measured ROS, the constraint set is convex and the modified CG algorithm is guaranteed to converge to the optimal constrained solution [12]. However, if we also constrain the magnitude response in the ROS, the constraint set is no longer convex and convergence to the optimal solution is not guaranteed. Nevertheless, our numerical experiments indicated no evidence of being trapped in a local minimum with this constraint [13].

The modified CG algorithm is given below:

Initialize:

$$h_0 = 0,$$
$$g_0 = \nabla f(h_0),$$
$$d_0 = -g_0$$

Do:

$$\alpha_k = \min_{\alpha} \phi(P(h_k + \alpha d_k))$$
$$h_{k+1} = P(h_k + \alpha_k d_k)$$
$$g_{k+1} = \nabla f(h_{k+1})$$
$$\beta_k = \frac{(g_{k+1} - g_k)^T g_{k+1}}{g_k^T g_k}$$
$$d_{k+1} = \beta_k d_k - g_{k+1}$$

until convergence criterion is satisfied.

We desire to rewrite (4) by taking the expectation, assuming a specific model for the autocorrelations of $s(n)$ and $u(n)$.

$$\phi(h) = \sum_n w(n) \left[\sum_k \sum_l (h(k) - \delta(k))(h(l) - \delta(l)) \right.$$
$$\times r_s(n-l, n-k) + \sum_k \sum_l (h(k))(h(l))$$
$$\times r_u(n-l, n-k) + 2\sum_k \sum_l (h(k) - \delta(k))(h(l))$$
$$\left. \times r_{su}(n-l, n-k) \right] \tag{5}$$

There are several ways of defining the models to be used for the correlation functions $r_u(k,l)$, $r_s(k,l)$, and $r_{su}(k,l)$ in the problem. Although complex models can be formulated for the correlation functions, we experimented with two simple autocorrelation models for the signal $s(n)$. The first was a simple uncorrelated model, and the second was a correlated autocorrelation model based on a first-order correlation [14] with a nonstationary variance. In both cases the measurement noise was assumed to be white (Gaussian), and the cross correlation between signal and noise was assumed to be zero. This means for
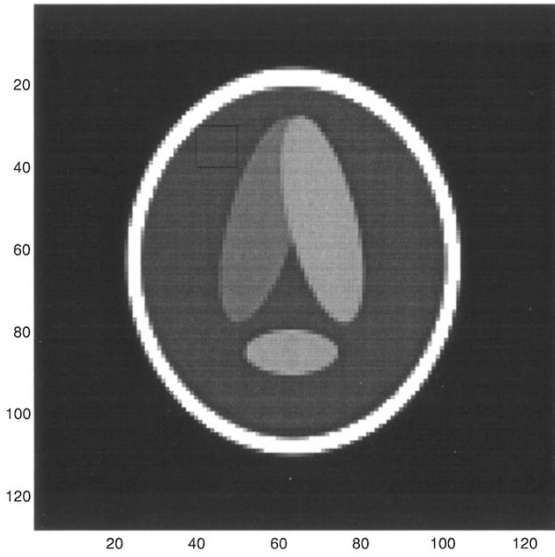
Fig. 6.   Original image with ROI shown.

the uncorrelated case

$$r_s(k,l) = E[s(k)s(l)] = \sigma_s^2(k)\delta(k-l) \tag{6}$$

$$r_u(k,l) = \sigma_u^2(k)\delta(k-l) \tag{7}$$

$$r_{\mathrm{su}}(k,l) = 0 \tag{8}$$

This model assumes no local correlation but allows the signal variance to vary from point to point. Using this model in (4) and evaluating the expected value, we get:

$$\phi(h) = \sum_n w(n)\left\{[h(n)-\delta(n)]^2 * \sigma_s^2(n) + \sigma_u^2(n) * h^2(n)\right\}. \tag{9}$$

The gradient of $\phi(h)$ is given by

$$\begin{aligned}
\frac{\partial\phi(h)}{\partial h(j)} &= \sum_n w(n)\left[2(h(j)-\delta(j))\sigma_s^2(n-j)\right.\\
&\qquad \left. + 2h(j)\sigma_u^2(n-j)\right]\\
&= 2(h(j)-\delta(j))\sum_n w(n)\sigma_s^2(n-j)\\
&\quad + 2h(j)\sum_n w(n)\sigma_u^2(n-j). \tag{10}
\end{aligned}$$

Simplifying (10) by writing the summation notation for the convolutions as convolution operators we obtain:

$$\begin{aligned}
\frac{\partial\phi(h)}{\partial h(j)} &= 2[h(j)-\delta(j)]\left[w(j)*\sigma_s^2(-j)\right]\\
&\quad + h(j)\left[w(j)*\sigma_u^2(-j)\right]. \tag{11}
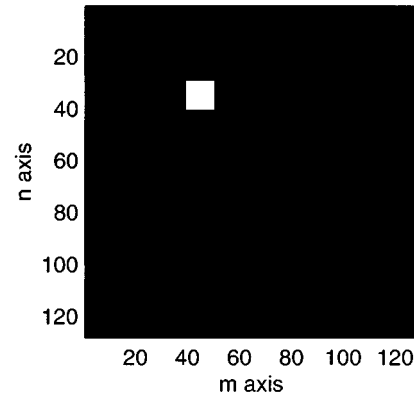\end{aligned}$$

Thus, we see that implementation of the gradient only requires convolution and pointwise signal multiplication. Other ways to ease the computational complexity, such as deriving an explicit form for the step size α in the CG method, can be found in [13].
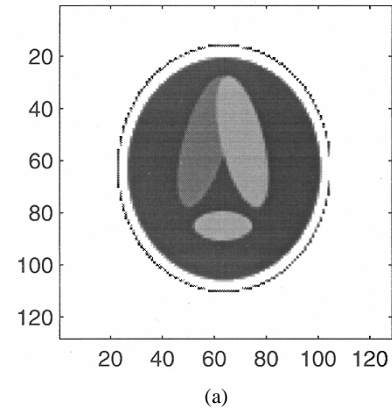
(a)
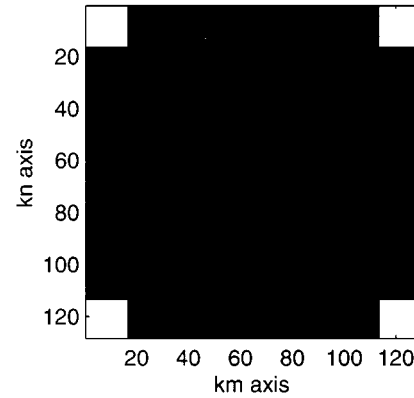
(b)

(c)

Fig. 7.   Design parameters.

The correlated signal model is a more accurate description of the statistics of most real-world images. For a correlated model we assume a signal correlation function with the following form:

$$r_s(k,l) = \sigma_s(k)\sigma_s(l)\rho^{|k-l|} \tag{12}$$

We use the same noise model (7) as for the uncorrelated case. For small ρ, the correlated signal model can be approximated as

$$r_s(k,l) = \sigma_s^2(k)\rho^{|k-l|} \tag{13}$$

Note that the approximate correlation model is formally invalid as a correlation function [14] but is retained due to its simplicity
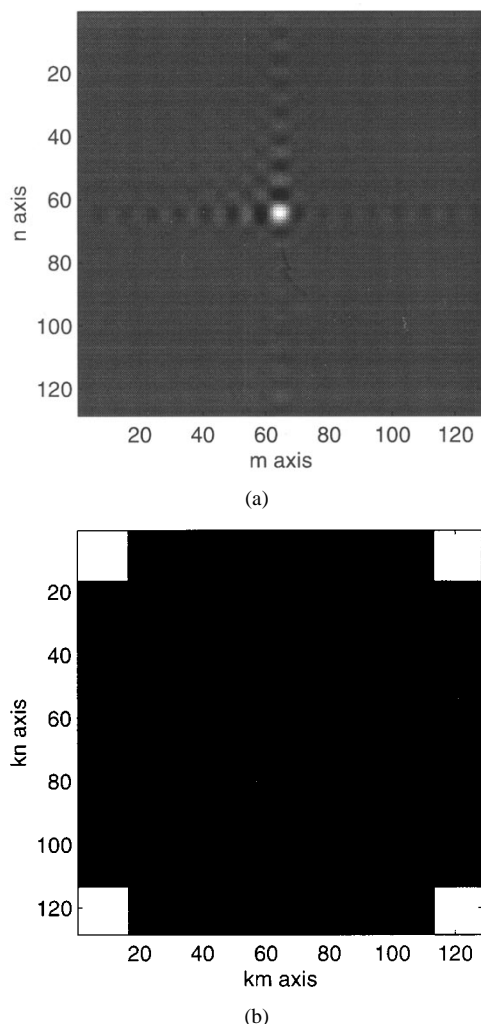
Fig. 8. Optimized filter as an image and its Fourier magnitude.

Fig. 9. (a) Image reconstructed with zeropadding and inverse FFT, (b) reconstructed image after applying h_{opt}.

of form and consequently its computational simplicity. The criterion is modified for the correlated model as:

$$
\begin{aligned}
&\phi(h) \\
&= \sum_n w(n) \left\{ \sum_k \sum_l [h(k) - \delta(k)][h(l) - \delta(l)] \right. \\
&\qquad \left. \times \sigma_s^2\,(n-k)\rho^{|k-l|} + \sum_k \sum_l h(k)h(l)\sigma_u^2(n-l)\delta(k-l) \right\} \\
&= \sum_n w(n) \left\{ \sum_k [h(k) - \delta(k)]\sigma_s^2(n-k) \right. \\
&\qquad \left. \times \sum_l [h(l) - \delta(l)]\rho^{|k-l|} + \sum_k h^2(k)\sigma_u^2(n-k) \right\}. \quad (14)
\end{aligned}
$$

The gradient is

$$
\begin{aligned}
\frac{\partial\phi(h)}{\partial h(j)} &= \sum_n w(n) \left\{ \sum_k \sigma_s^2(n-k)[h(k) - \delta(k)]\rho^{|k-j|} \right. \\
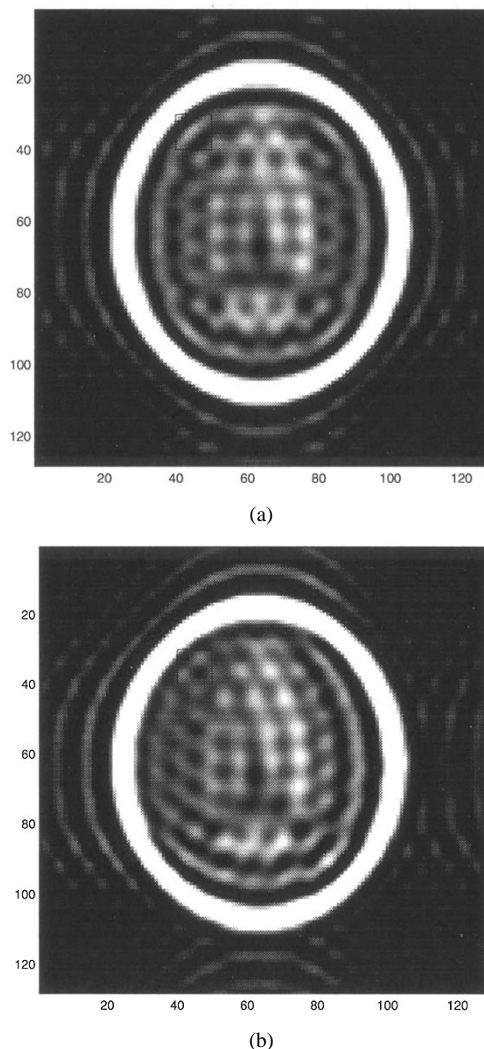&\qquad \left. + \sum_l \sigma_s^2(n-j)[(h(l) - \delta(l))]\rho^{|j-l|} \right\}
\end{aligned}
$$

$$
\begin{aligned}
&\qquad + 2h(j)\left[w(j) * \sigma_u^2(-j)\right] \\
&= \left\{ [w(j) * \sigma_s^2(-j)]\,[h(j) - \delta(j)] \right\} * \rho^{|j|} \\
&\quad + [w(j) * \sigma_s^2(-j)] \left\{ [h(j) - \delta(j)] * \rho^{|j|} \right\} \\
&\quad + 2h(j)\left[w(-j) * \sigma_u^2(j)\right]. \quad (15)
\end{aligned}
$$

The result in the correlated model case is a complicated gradient expression that can not be implemented as convolutions and hence is computationally inefficient when compared to the gradient form derived for the uncorrelated case.

C. 1-D Simulations

Some issues arising in this design method are more easily visualized in 1-D. Therefore, we begin with a set of 1-D simulations and follow this with 2-D simulations where that is more appropriate.

1) Resolution: For our standard approach, we constrained the Fourier magnitude to be constant in the ROS and zero elsewhere. We chose to impose a constant constraint so that the result would be less sensitive to the exact location of the ROI and
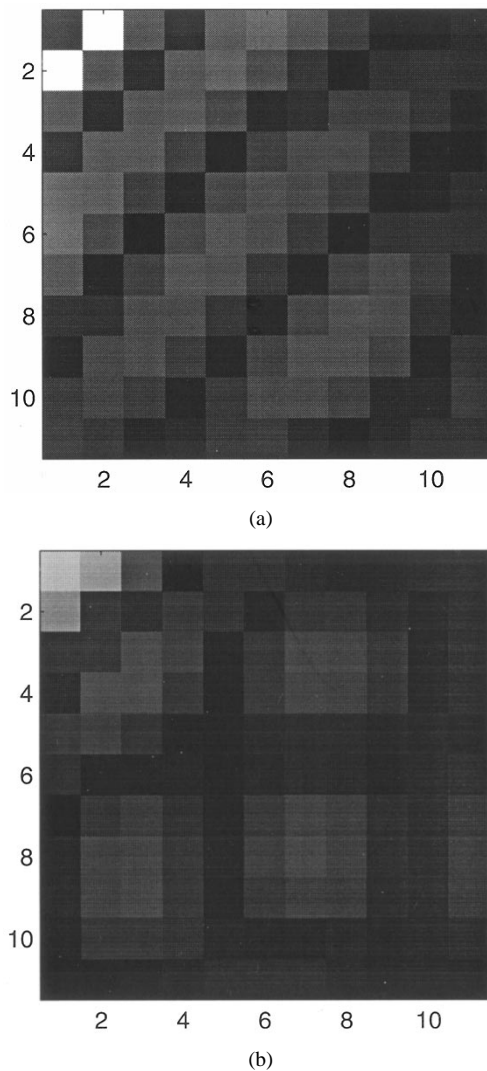
(a)

(b)

Fig. 10.   Absolute error in ROI.

(a)

(b)

Fig. 11.   Circular ROS: Optimized filter as an image and its Fourier magnitude.

the exact values of relative variances assumed in different regions of the image. If the ROI includes a region very close to the interfering signal, a constant magnitude tends to be best since the mainlobe width is approximately preserved; that is, ringing is reduced but not at the expense of a loss of resolution. To see this, we did a simple comparison with a 1-D design problem.

The signal standard deviation in this case was defined to be 40 in the weak signal region and 800 in the strong signal region and the noise variance is unity. The ROI is also shown and was defined to be between points 15 and 25, which is close to the stronger region of the signal. The results for this case are shown in Fig. 2.

Also shown in Fig. 2 is the magnitude and the phase of the Fourier transform of h_{opt}. Note that the magnitude satisfies an ideal LPF as designed. Also note how the sidelobes are smaller on one side of the designed filter to reduce the error associated with sidelobes when the designed filter is convolved with a signal that has the variance characteristics defined.

To see that resolution has not been sacrificed, we plotted an interpolated version of the designed PSF along with the original PSF. A visual inspection shows that the mainlobe width of the designed PSF is almost exactly the same as that of the original
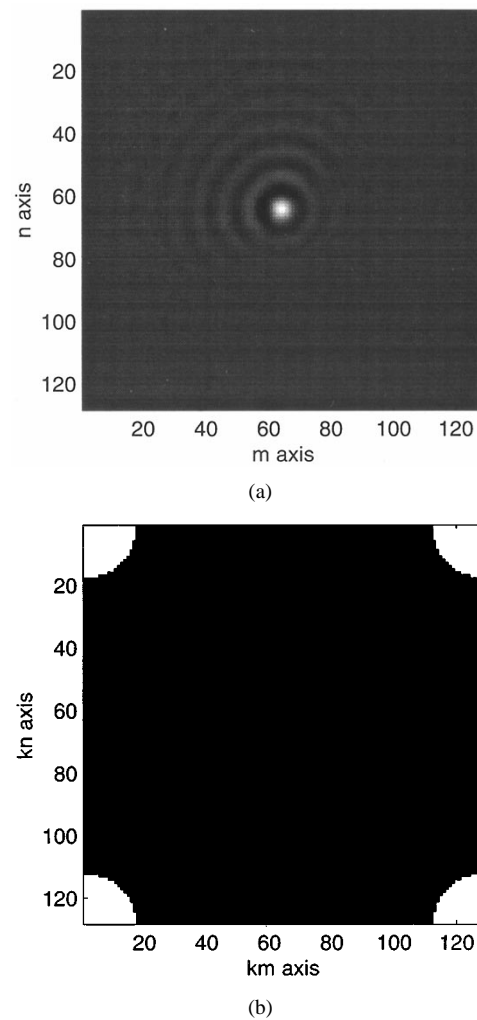
PSF in Fig. 3. Measurements show that the full-width half-max (FWHM) resolution is 5.25 samples in the original and 5.5 samples in the designed PSF. Thus, the primary gains in the PSF design come from steering the ringing away from the ROI. This behavior is representative of the results observed in all our simulations.

2) Correlated and Uncorrelated Model Comparison: We consider now whether the extra computation and complexity required for the correlated case is justified by superior results. To compare the filter designed from the correlated and uncorrelated correlation models we consider the same design problem as discussed previously. The same parameters were used for the correlated case but with a correlated autocorrelation model for s with $\rho = 0.5$. The resulting filter is shown in Fig. 4.

The main difference in the result is that the central lobe of the filter increases slightly in magnitude (by 0.007) and becomes slightly narrower. There is little change in the sidelobes between the correlated and the uncorrelated model. This result illustrates that using the correlated autocorrelation model provides little improvement in reducing the sidelobes or modifying the mainlobe, while the computational complexity has increased significantly. Further experiments confirmed this observation [13].

3) Magnitude Constraint Effect: The constraint can be a nonlinear constraint (an ideal LPF with unity gain in the
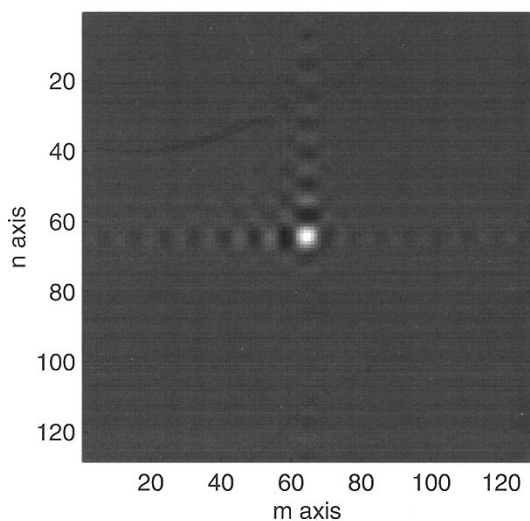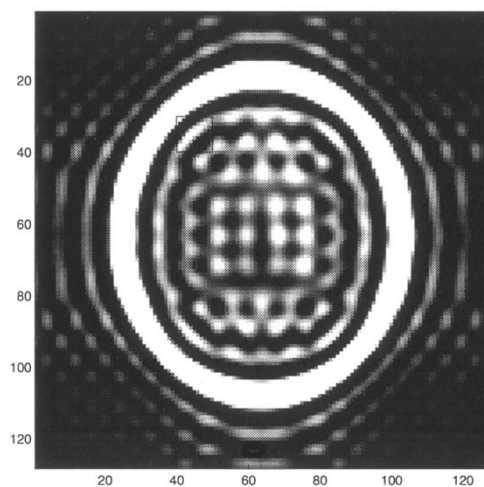
(a)
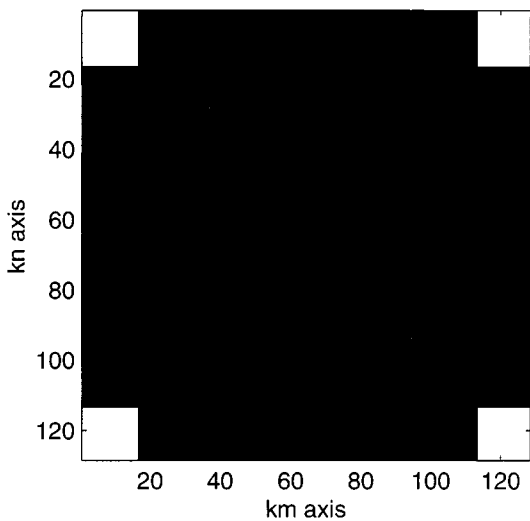
(b)

Fig. 12. Variance effect: Optimized filter image and Fourier transform magnitude of h_{opt}.

(a)

(b)

Fig. 13. Variance effect: (a) image reconstructed with zeropadding and inverse FFT, (b) reconstructed image after applying h_{opt}.
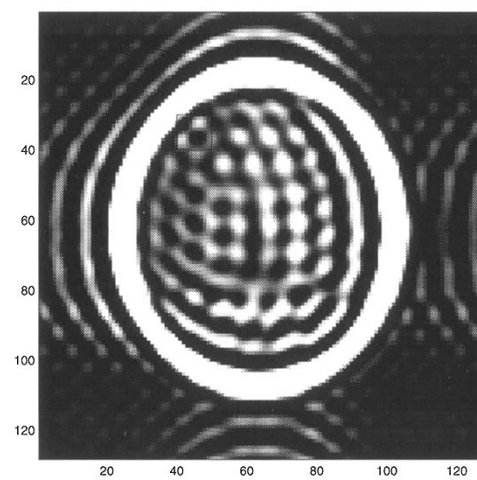
frequency ROS) or a linear constraint (zero response outside the passband). The linear constraint does not impose the unity gain requirement and thus a rolling-off effect is allowed for the magnitude of the Fourier transform of h_{opt} as seen in Fig. 5. This rolling-off effect means that the sidelobes can be made smaller, leading to less error associated with sidelobes. The peak value is decreased slightly because forcing the PSF to be smaller makes the error term associated with ringing from outside the ROI smaller at the expense of more error in the relatively small signal matching term.

D. 2-D Simulations

1) Baseline 2-D Simulation: We used the digital head phantom shown in Fig. 6 to test our method on a 2-D problem. This was considered to be the high-resolution original image. The ROI in the image is marked by a small square. We assumed that the data from a 32×32 lowpass k-space region around the origin was available for reconstructing the image. This data was used to reconstruct (interpolate) the image on a 128×128 grid.

If we reconstruct using the standard approach of zeropadding the frequency domain to 128×128 and taking an inverse FFT, we obtain the image shown in Fig. 9(a).

We designed a postprocessing filter to improve this result in the ROI. We assumed a known relative local standard deviation map of the signal as shown in Fig. 7. The ratio of the stronger signal standard deviation in the scalp to the weaker signal standard deviation in the ROI was 10. Note that the standard deviation image model used in this case differs from that of a typical MRI scan in that we assumed large signal standard deviation outside the head. This is simply a design technique we used to emphasize that interference from the outer ring is what we are trying to minimize; that is, the main goal is to prevent interference from outside of the brain into the ROI rather than interference from other parts within the brain.

Using these assumptions, we designed the filter by minimizing (9) under the constraint that the Fourier magnitude is constant in the ROS and zero elsewhere. As mentioned previously, if the ROI includes a region very close to the interfering signal, a constant magnitude tends to be best since the mainlobe width is approximately preserved. However, if the ROI is farther away from the interfering signal, it is better
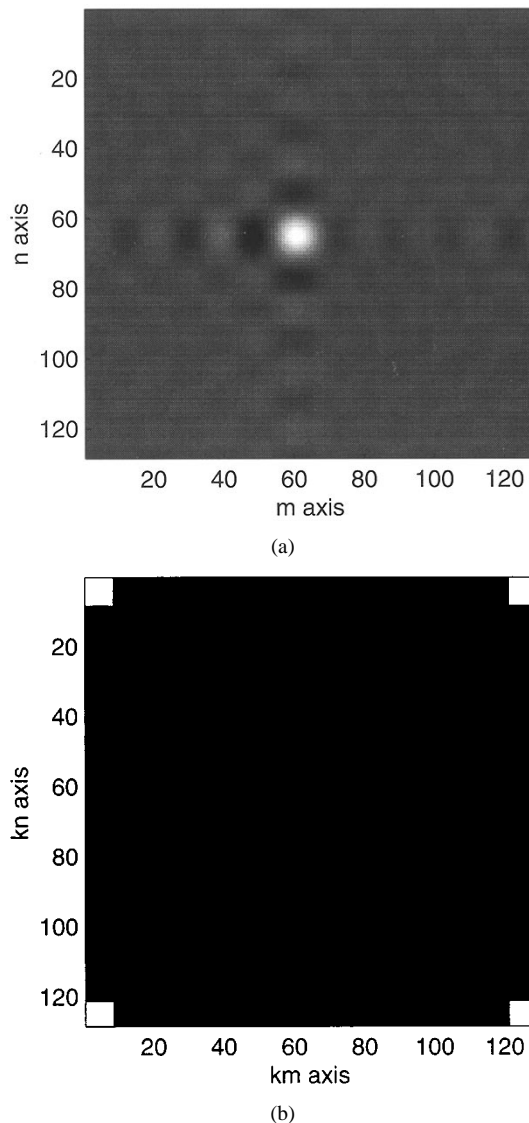
(a)

(b)

Fig. 14.   ROS definition effect: Optimized filter image and Fourier transform magnitude of h_{opt}.

(a)

(b)

Fig. 15.   ROS definition effect: (a) image reconstructed with zeropadding and inverse FFT, (b) reconstructed image after applying h_{opt}.

to apodize the frequency response to reduce the effect of tails at the expense of a broader mainlobe. The constant magnitude constraint can easily be relaxed if a more case-specific result is desired. The resulting optimized filter is shown as an image along with its Fourier magnitude in Fig. 8. Note that in this case the optimized filter is asymmetric along both axes since the ROI is close to the upper and left sides of the outer ring. Thus, there are two possible directions that can ring into the ROI. As the design requires, the Fourier transform of h_{opt} matches the ROS defined in the problem.

To show that the designed filter indeed reduces the ringing in the ROI, consider the original image shown in Fig. 6 (with the ROI marked by a small square). After reconstructing the image with the optimal filter response h_{opt}, we obtained the image shown in Fig. 9(b). The MSE for the LPF image ROI was $5.78e5$ and for the optimized image ROI was $1.94e5$, a 66% reduction. The absolute error (defined as $error = |original - filtered|$) between the original and the two filtered images is shown as an image in Fig. 10 in the ROI. In these images the whiter a pixel
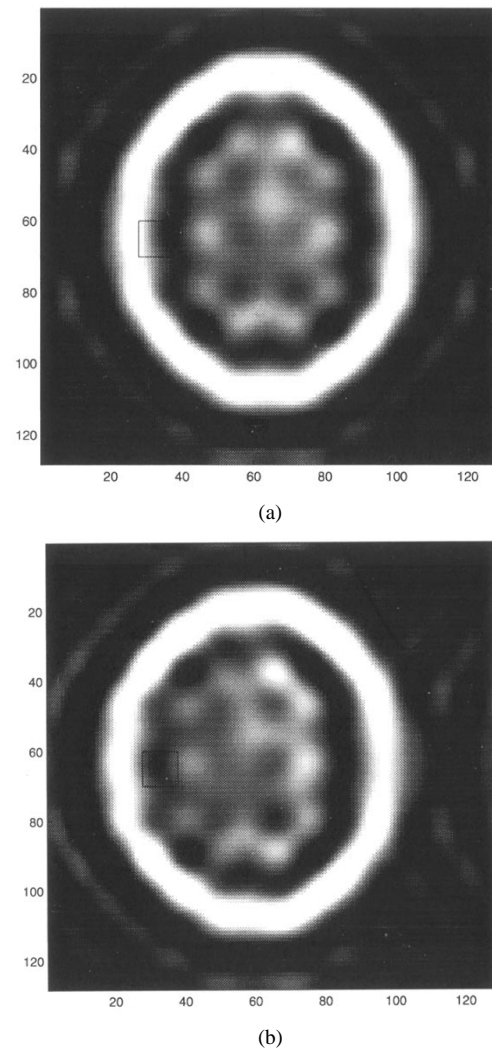
is, the larger the error is. Note that these images are displayed with the same intensity scale.

2) Circular ROS: In this case we modified the previous example so that the ROS is circular instead of rectangular and all other parameters were the same. The resulting optimized filter exhibits in this case circular asymmetry along the diagonal axis as shown in Fig. 11. The MSE for the LPF ROI was $5.44e5$ and for the optimized ROI was $1.95e5$, a 64% reduction.

3) Effect of Variance: As the strength of the outer signal from the scalp becomes stronger, it becomes more difficult to reduce the effect of the ringing. In this case we considered a relative standard deviation of 20 between the signal in the ROI and the stronger signal. The other parameters were left the same as the baseline case. The optimized filter is shown in Fig. 12 with the Fourier transform magnitude of the designed filter. Note how the designed filter is slightly more asymmetric than in Fig. 8 since the relative variance is larger. The sidelobes decay even faster on one side to try to reduce the interference from the strong signal region.

The LPF image and the image after applying the designed filter are shown in Fig. 13. The MSE in this case was $4.68e6$ and for the optimized image $1.87e6$, a 60% reduction. We see that
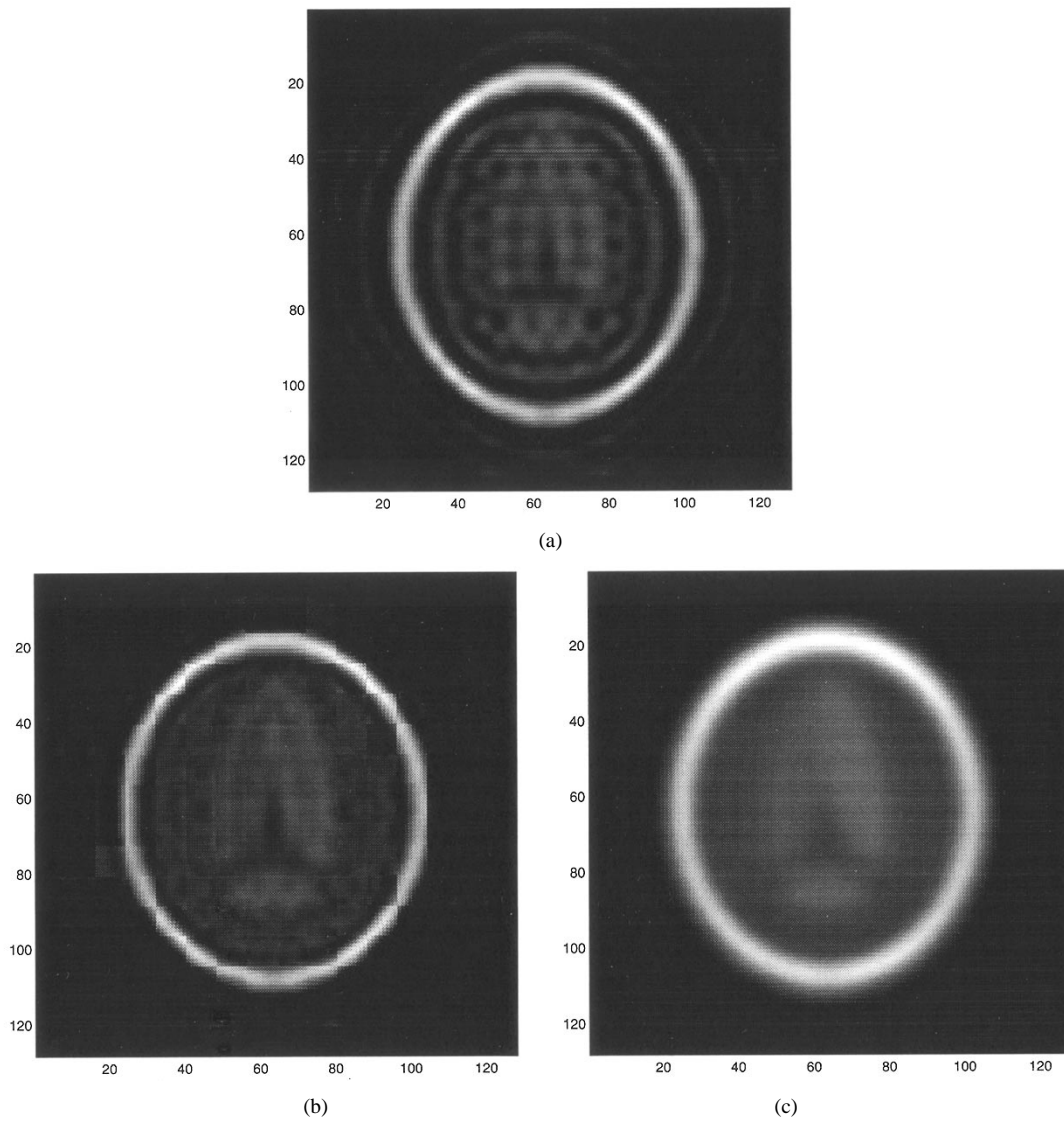
Fig. 16.   (a) Lowpass image, (b) Composite optimized image, and (c) Image reconstructed with Hamming window.
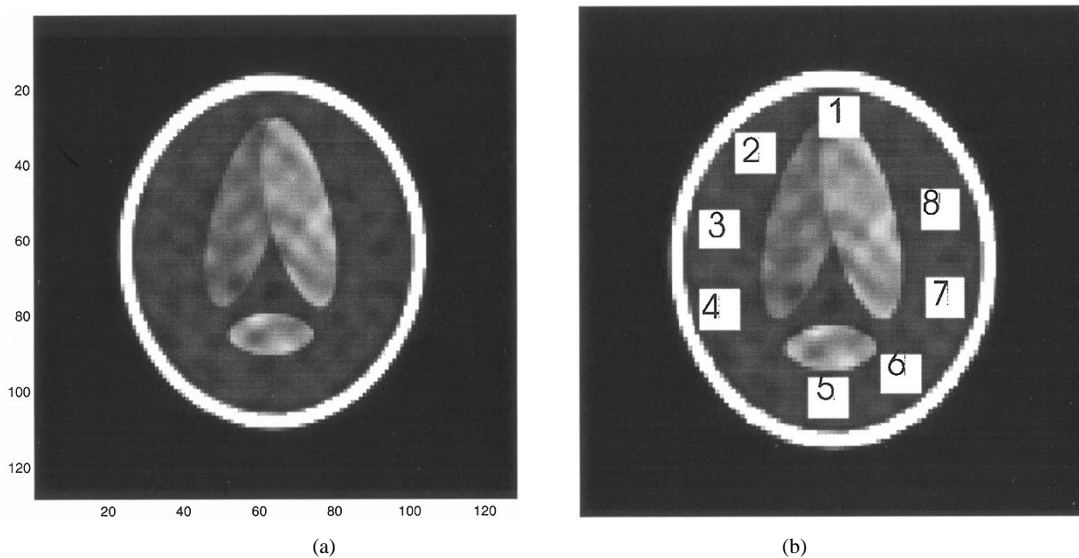

Fig. 17.   (a) Original image and (b) regions for concentration measurements.

the MSE increased since there was a larger amount of ringing, but the designed filter still managed to reduce it. Our exper-iments show that increasing the relative variance beyond the value used in this example does not yield significantly different
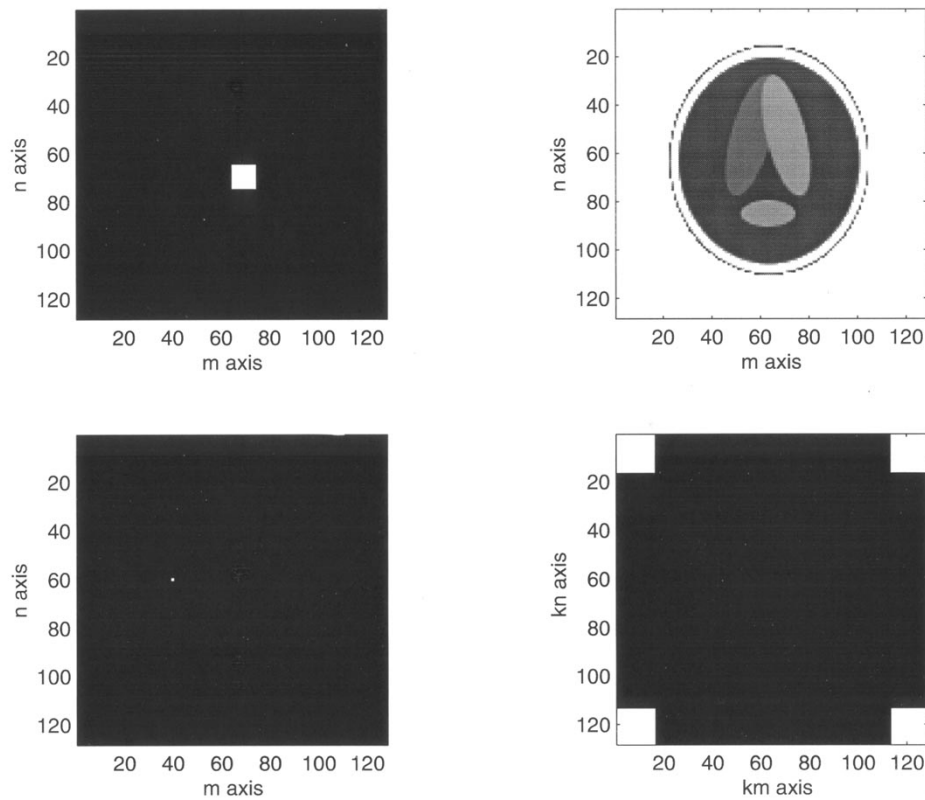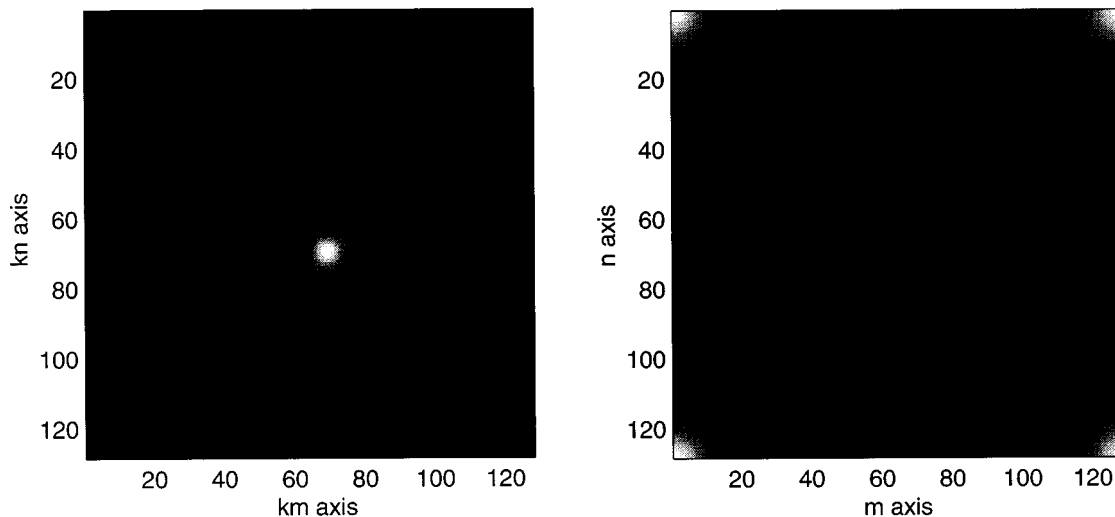
Fig. 18.   Design parameters.

Fig. 19.   Optimized filter image.

filter shapes. This justifies our claim that the relative strength of the signals is not critical as long as one is much larger than the other.

4) Effect of ROS Definition and ROI Location: The ROS is specified to match the way in which the frequency samples for the image were acquired. The fewer samples obtained, the more the image manifests ringing and blurring. In this simulation, we reduced the size of the ROS by half to see the effect it has on the performance of the designed filter. We also defined an ROI that has ringing influence mainly from one side to show how the design procedure adapts to such a case. Intuitively, one would

expect worse performance since more ringing is unavoidable. The optimized filter image is shown Fig. 14. The MSE for the LPF image was $1.29e6$ and for the optimized image $1.75e5$, an 86% improvement. The original image after the LPF and the result after LPF and filtering with h_{opt} are shown in Fig. 15. The increased blurring and ringing is evident in both images; however, the filtered image ROI is a significant improvement over the unfiltered image.

5) Composite Image: A composite reconstructed image was formed as follows. The image was divided into 8×8 blocks, each of which was considered one at a time to be the ROI. An
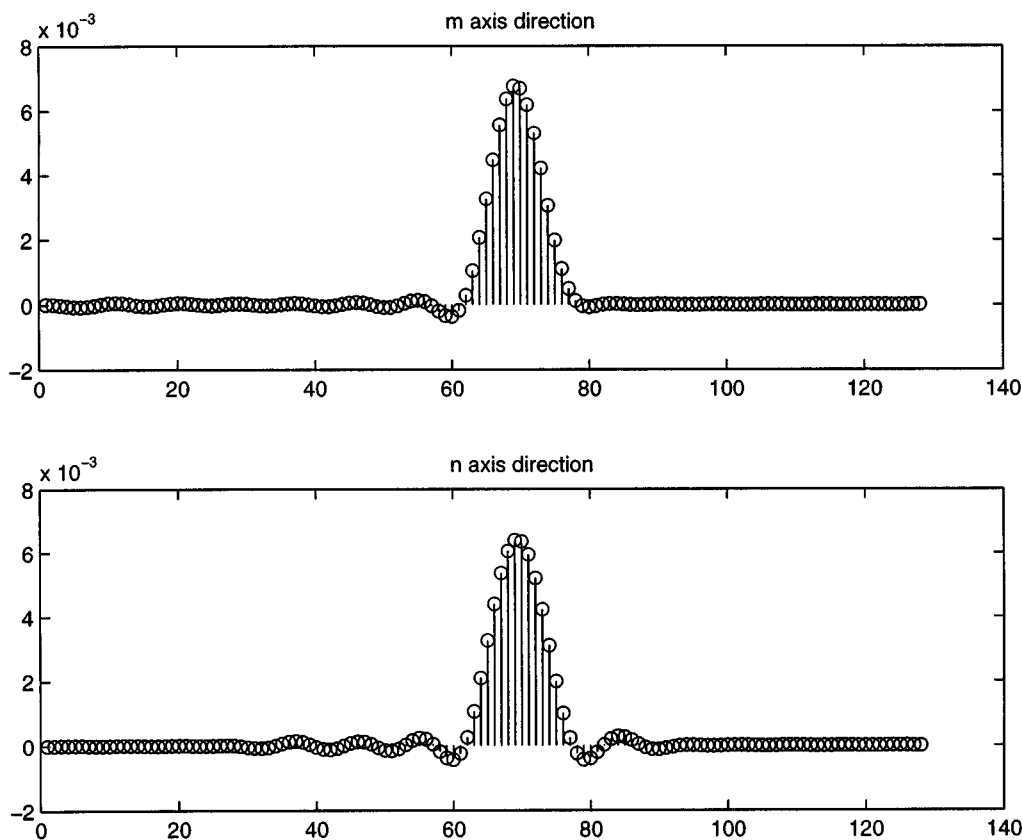
Fig. 20. Optimized filter cross section plot.

TABLE I
COMPARISON OF CONCENTRATION ESTIMATES

Region	Concentration				MSE		
	Original	Optimized	LPF	Hamming	Optimized	LPF	Hamming
1	109.91	101.38	101.21	133.07	72.87	75.66	536.29
2	74.45	69.32	72.13	85.42	26.40	5.39	120.34
3	71.52	68.29	58.51	68.73	10.43	169.26	7.80
4	69.71	63.88	61.38	70.53	33.98	69.46	0.66423
5	63.76	63.66	50.33	127.96	0.01	180.29	4121.60
6	67.91	66.00	66.83	229.95	3.65	1.16	26258.00
7	67.07	69.82	55.58	157.82	7.55	132.11	8236.30
8	70.97	72.36	64.28	89.42	1.95	44.77	340.44
					Avg = 19.60	Avg = 84.76	Avg = 4952.70

optimized filter was designed for each ROI, and then the image was reconstructed with the optimized filter.

The ROI's were extracted from each reconstructed image obtained by filtering the lowpass image in Fig. 16(a) and then were put together to form a composite image. The resulting image is shown in Fig. 16(b). For comparison purposes an image was reconstructed using a Hamming window to roll off the frequency response. The result is shown in 16(c). While there is significantly less ringing in the Hamming reconstruction, the result is obtained at the expense of a significant loss of resolution. On the other hand, the optimized reconstruction has significantly less ringing than the original lowpass reconstruction but without any noticeable loss of resolution. However, blocking artifacts are apparent in the optimized reconstruction. A more sophisticated method could easily be developed to interpolate between blocks or overlap blocks so that no blocking artifact occurs, but

we have not explored that in this paper. While the composite image is useful for understanding and comparing our method to others, the primary value of the method as proposed here is to reconstruct a small ROI more faithfully rather than improve an entire image.

III. FILTER DESIGN FOR MEASURING CONCENTRATION

A. Criterion

In the previous section, we designed a filter with the goal of reducing ringing in a given region. Our interest in this section is to design a filter that minimizes the effects of ringing and at the same time acts as an averaging kernel to measure the concentration in a given region. We observe that convolution can be used to find the local average of a certain region. The kernel acts as a moving average mask. Thus each pixel of the resulting image
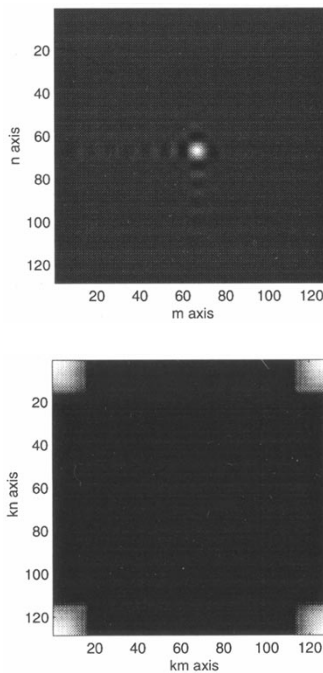
Fig. 21.   Averaging kernel size effect: Optimized filter image.

after convolution is an average of a corresponding region of the original image. The concepts developed earlier can be modified by interpreting the problem as designing a filter that will match the averaging kernel instead of an impulse as closely as possible while satisfying the imposed constraint. That means (4) is modified to be:

$$\phi(h(n)) = \sum_{n} w(n)[E(\{[h(n) - h_{\mathrm{avg}}(n)] * s(n)\}^2$$
$$+ [h(n) * u(n)]^2$$
$$+ 2(\{[h(n) - h_{avg}(n)] * s(n)\}[h(n) * u(n)]))]. \tag{16}$$

where $h_{\mathrm{avg}}(n)$ is the averaging kernel that we are trying to match now. The weighting function $w(n)$ is chosen as a delta function at the location in the average image where the average is desired. As previously explained, the constraint can be either linear or nonlinear. However, since the final objective is not an image for visual inspection we use a linear constraint. The reason for this is that the linear constraint allows the rolling off of the Fourier transform magnitude; thus, the sidelobes will be smaller than with a nonlinear constraint. We could also choose to enforce a magnitude constraint equal to the product of the ROS and the Fourier transform magnitude of the ideal averaging kernel. The expected results should again exhibit the asymmetric behavior that attempts to reduce the ringing into the region where we are trying to measure the concentration.

B. Simulations

To demonstrate the effectiveness of optimized filtering, consider the synthetic image shown in Fig. 17(a). This image attempts to simulate the varying intensities in the concentration of an MRI image. We consider this image to be the original. As in the previous simulations, we defined the ROI (a single
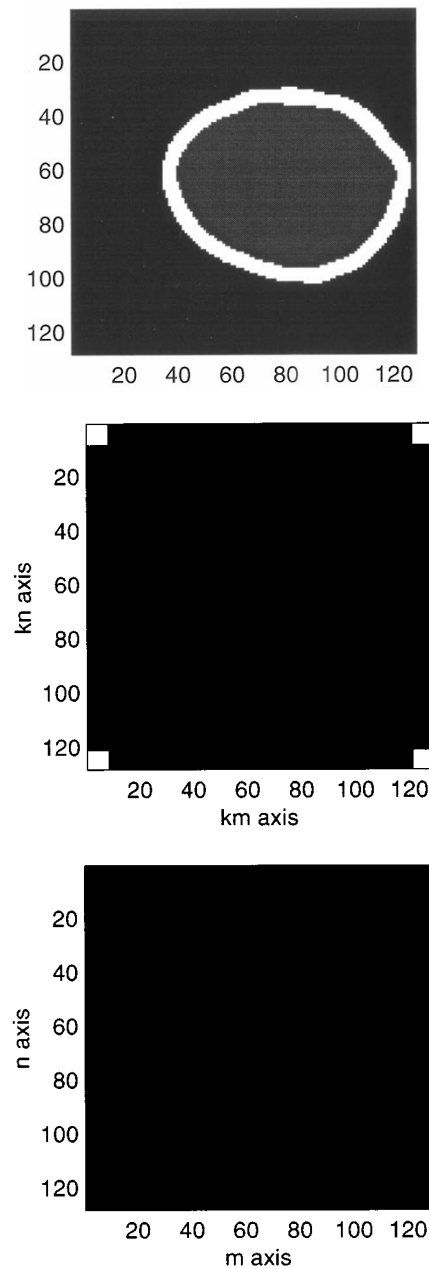

Fig. 22.   Design parameters.

point that samples the averaged image), the signal standard deviation image which has a relative standard deviation of 10, the measurement noise standard deviation of 1, and the size of the averaging kernel of 10×10. We computed an optimized filter to compute concentration in each of the eight different 10×10 regions shown in Fig. 17(b). The prior information assumed for Region 3 is shown in Fig. 18.

We show in Fig. 19 the optimized filter as an image with its Fourier transform magnitude for computing the concentration of Region 3. Note that this time the Fourier transform magnitude is no longer that of an ideal LPF, but rather there is a rolling off of the edges. Since the rolling off in this case reduces the sidelobes very rapidly, for better visibility we plot a cross section of the optimized filter along its two axes as shown in Fig. 20. As can be seen from the plots, the designed filter is mainly asymmetric along the m axis. This is because the optimized filter is
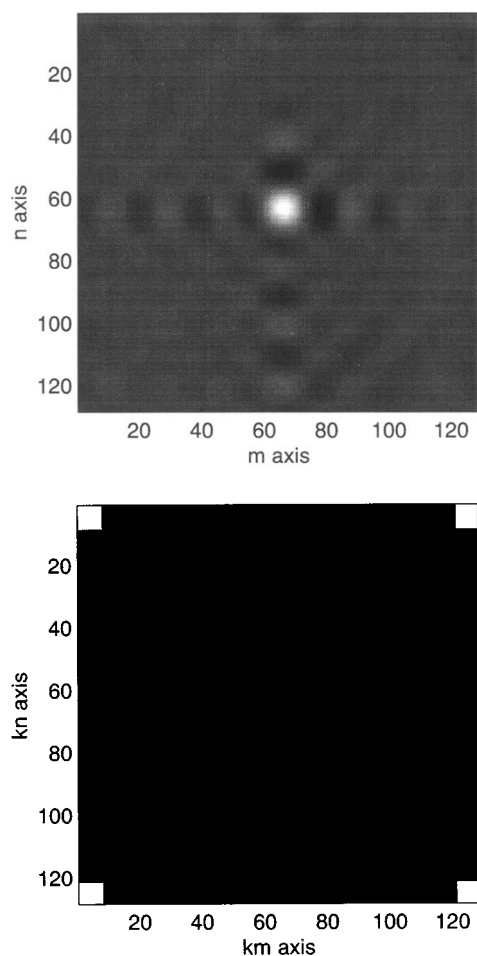
Fig. 23. Optimized filter as an image and its Fourier magnitude.

Fig. 24. (a) Image reconstructed with zeropadding and inverse FFT, (b) reconstructed image after applying h_{opt}.

attempting to reduce the ringing primarily from the left side of the outer ring.

Concentration was calculated using the original image, and estimates were made using the lowpass image before postprocessing and the same image after postprocessing with the appropriate optimized filter. On average, the optimized filter did a better job of estimating the concentration, since it reduced the amount of ringing from the outer edges. For comparison purposes, concentration was also estimated from an image reconstructed using a Hamming window to reduce ringing artifacts. Once again, the optimized filter outperformed the results using the Hamming window apodization. The blurring introduced by apodization introduces significant error in the concentration estimates near the large outer signal. Numerical results are given in Table I.

IV. POSTPROCESSING OF EXPERIMENTAL DATA

To further demonstrate the effectiveness of the developed method we tested it on experimental data provided to us courtesy of the Center for Nuclear Imaging Research at the University of Alabama at Birmingham. The data was from a 32×32 set of k-space samples centered around the origin acquired from an NAA image. This data was used to reconstruct (interpolate) the image onto a 128×128 grid, and we used it
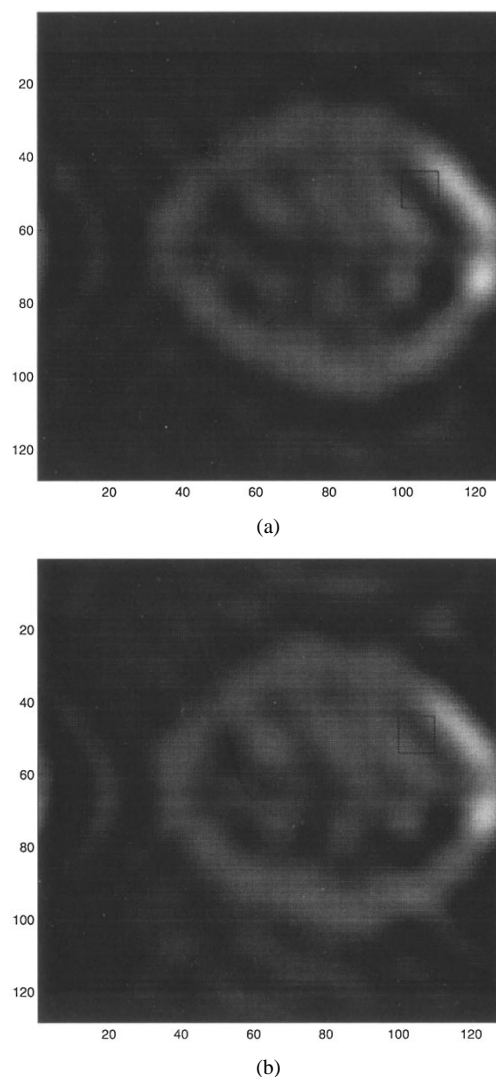
as a basis for a manually constructed model for the standard deviation image shown in Fig. 22.

The resulting optimized filter with the Fourier transform magnitude is shown in Fig. 23. We again see the asymmetric behavior exhibited in the previous examples. As done in the previous cases, we show the standard image reconstructed by zeropadding the frequency domain to 128×128 and taking an inverse FFT and the image resulting from applying h_{opt} in the postprocessing. These images are shown in Fig. 24. Notice that the optimized image does not contain as deep a dark ring near the large scalp signal. The negative sidelobe has been significantly suppressed, so that the signal inside the brain is more uniform as expected.

V. CONCLUSION

The method we have developed here is able to reduce significantly the interference of a large unwanted signal in a nearby ROI. It does not require restrictive assumptions about the image such as having a limited spatial ROS or consisting of homogeneous regions. Furthermore, it is not sensitive to the exact locations of edges or exact knowledge of the local strength of the

signal and noise. Once a filter has been designed it can be used for any image with the same requirements for ringing orientation. There is no need to design a new filter for each image in a given acquired set or to perform accurate segmentation. This is particular advantageous in MRSI, where a set of spectral images of the same object must be reconstructed. The method can also be adapted to measuring concentration in a region with minimum MSE rather than reconstructing a region with minimum MSE. The computational simplicity of our method is due to the fact that the filter design process need not be repeated for each image in an acquired set since it is not particularly sensitive to small variations in the prior information used to derive the filter. In addition, the filter can be implemented efficiently by the use of FFT's.

An extension is also possible for reconstructing entire brain images with minimal interference from the scalp signal. This could be done by designing several filters with different orientations, reconstructing an image for each orientation, and then selecting each pixel from the image in which the interference is steered away most from that pixel location. This, of course, would require several FFT's but may be more efficient than iterative nonlinear restoration methods.

REFERENCES

[1] Z. H. Cho, J. P. Jones, and M. Singh, *Foundations of Medical Imaging*: Wiley, 1993.

[2] T. F. Kirn, "Magnetic resonance spectroscopy may hold promise in studying metabolites, tissues," *J. Amer. Med. Assoc.*, vol. 261, p. 1103ff, 1989.

[3] P. R. Luyten *et al.*, "Metabolic imaging of patients with intracranial tumors: H-1 MR spectroscopic imaging and PET," *Radiology*, vol. 176, pp. 791–799, 1990.

[4] D. L. Arnold *et al.*, "Proton magnetic resonance spectroscopic imaging for metabolic characterization of demyelinating plaques," *Annals of Neurology*, vol. 31, no. 3, pp. 235–241, 1992.

[5] W. J. Chu, H. P. Hetherington, R. I. Kuzniecky, T. Simor, G. F. Mason, and G. A. Elgavish, "Lateralization of human temporal lobe epilepsy by 31P NMR spectroscopic imaging at 4.1 T," *Neurology*, vol. 51, pp. 472–479, Aug. 1998.

[6] S. Plevritis and A. Macovski, "Spectral extrapolation of spatially bounded images," *IEEE Trans. Med. Imag.*, vol. 14, pp. 487–497, Sept. 1995.

[7] X. Hu, D. N. Levin, P. C. Lauterbur, and T. A. Spraggins, "SLIM: Spectral localization by imaging," *Magnetic Resonance in Medicine*, vol. 8, pp. 314–322, 1988.

[8] Z. Liang and P. C. Lauterbur, "A generalized series approach to MR spectroscopic imaging," *IEEE Trans. Med. Imag.*, vol. 10, pp. 132–137, June 1991.

[9] E. M. Stokely and D. B. Twieg, "Functional image reconstruction enhancement (FIRE) for MR spectroscopic and nuclear medicine images," *SPIE Med. Imag. VI*, 1992.

[10] R. R. Schultz and R. L. Stevenson, "A Bayesian approach to image expansion for improved definition," *IEEE Trans. Image Process.*, vol. 3, pp. 233–242, May 1994.

[11] R. L. Lagendijk, R. M. Mersereau, and J. Biemond, "On increasing the convergence rate of regularized iterative image restoration algorithms," in *Proc. 1987 IEEE Int. Conf. Acoustics, Speech, and Signal Processing*, pp. 1183–1186.

[12] R. Marucci, R. M. Mersereau, and R. W. Schafer, "Constrained iterative deconvolution using a conjugate gradient algorithm," in *Proc. 1982 IEEE Int. Conf. Acoustics, Speech, and Signal Processing*, pp. 1845–1848.

[13] T. Bakir, "A filter design method for minimizing blur in a region of interest in low-resolution MRI images," Master's thesis, Auburn University, 1998.

[14] A. K. Jain, "Advances in mathematical models for image processing," *Proc. IEEE*, vol. 69, pp. 502–528, May 1981.